

## Article

# Early-Age Properties Evaluation of Nano-Metakaolin Cement Paste Based on Electrochemical Impedance Spectroscopy

Qiuchao Li, Yingfang Fan \*, Yulong Zhao and Zilong Liang

Institute of Road and Bridge Engineering, Dalian Maritime University, Dalian 116026, China

\* Correspondence: fanyf@dlmu.edu.cn

**Abstract:** The early-age properties of nano-metakaolin (NMK) cement paste were examined from 15 min to 24 h, contacted between cement and water based on the electrochemical impedance spectroscopy (EIS) method. The effects of a superplasticizer and chloride ions were taken into consideration. The variation of the electrochemical parameters of NMK cement paste with or without the superplasticizer and chloride ions was analyzed. The results demonstrated that the solution resistance and impedance modulus of the cement paste decreased first then increased between 15 min and 12 h after cement contact with water. When the cement contacted with water within about 8 h, the pore solution resistance and impedance modulus were less affected by NMK. When the cement hydration was over about 8 h, the pore solution resistance and impedance modulus of the cement paste were significantly improved by the addition of 1% NMK. The pore solution resistance of the cement paste with 1% NMK was increased by 0.49%, 2.64% and 18.17% as compared with ordinary cement paste when the hydration time was 4 h, 8 h and 12 h, respectively. NMK promoted cement hydration and increased the pore solution resistance and impedance modulus in the cement paste with or without the superplasticizer and chloride ions. The superplasticizer and chloride ions reduced the pore solution resistance and impedance modulus of cement paste with or without NMK.



**Citation:** Li, Q.; Fan, Y.; Zhao, Y.; Liang, Z. Early-Age Properties Evaluation of Nano-Metakaolin Cement Paste Based on Electrochemical Impedance Spectroscopy. *Buildings* **2022**, *12*, 1763. <https://doi.org/10.3390/buildings12101763>

Academic Editor: Abdelhafid Khelidj

Received: 22 September 2022

Accepted: 17 October 2022

Published: 21 October 2022

**Publisher's Note:** MDPI stays neutral with regard to jurisdictional claims in published maps and institutional affiliations.



**Copyright:** © 2022 by the authors. Licensee MDPI, Basel, Switzerland. This article is an open access article distributed under the terms and conditions of the Creative Commons Attribution (CC BY) license (<https://creativecommons.org/licenses/by/4.0/>).

**Keywords:** nano-metakaolin; electrochemical impedance spectroscopy; cement paste; pore solution resistance; impedance modulus

## 1. Introduction

To improve the mechanical properties, durability and self-cleaning function of cement-based materials, nanomaterials such as nano clay, carbon nanotubes, nano SiO<sub>2</sub> and nano TiO<sub>2</sub> have been incorporated into cement-based materials. However, the productivity cost was higher for carbon nanotubes, nano-silica, etc. [1–4]. Nano-metakaolin (NMK) is pollution-free in the production process, and the raw material of NMK is abundant. Additionally, it can meet the requirements of the mechanical properties and durability of cement-based materials by controlling the production process, and NMK attracts more attention [5–9]. Nano-metakaolin is made from nano-kaolinite clay which is milled after high-temperature (500–900 °C) calcination [5,6]. Due to the filler effect, the nucleation effect and the pozzolanic activity of NMK, the internal pore structure of cement-based materials is refined and achieves the excellent mechanical and durability properties of cement-based materials [7–9]. Furthermore, a low addition (0.5–1% by mass of cement) of nano-metakaolin effectively increases the viscosity and yield stress of fresh cement paste; however, the rate of structural build up is weakened by the over addition (1.3%) of nano-metakaolin [10]. A small amount (1% by mass of cement) of nano-metakaolin is enough to perform the pozzolanic reaction and filler effect, generate more C-S-H, refine the internal pore structure of concrete, and improve the strength of concrete [11]. To date, more attention has been paid to the rheological performance, mechanical properties and durability properties of NMK cement paste. However, the early-age hydration and electrochemical properties have not been clear, which limits the application of cement-based materials with nano-metakaolin addition to practical engineering.

Electrochemical impedance spectroscopy (EIS) is an approach that uses low-amplitude sinusoidal voltages to perturb the electrochemical system to be tested, which aims to obtain electrochemical parameters [12,13]. During EIS testing, a small amplitude of a sinusoidal voltage is applied to the system under test, which aims to reduce the perturbation of the applied voltage to the system under test [14]. In fresh cement paste, the structure generated by cement hydration is a microscopic porous medium. Keddam et al. [15] have successfully applied the electrochemical impedance spectroscopy method in the field of cement-based materials. The materials are considered to be a special chemical system, i.e., an electrolyte solution system, and electrolyte solution is present in the pore structure. Fresh cement paste is an electrical conductor and can be seen as an equivalent circuit with a series of resistances, capacitances and inductors, and its electrical impedance response is affected by the pore structure network [16]. The measurement of EIS is influenced not only by the solid part and pore structure of the cement paste, but also by the conductivity of the pore/interstitial solution [17]. AC impedance spectra can be used to obtain the hydration state and microstructural parameters of the cement paste [17,18]. For the investigation of the conductivity of cement-based materials, EIS can reduce the phenomenon of ion directional movement in the pore solution and improve the accuracy of the impedance test which is compared with the direct current testing method. The electrochemical parameters obtained by EIS can also reflect the variation of the internal pore structure and mechanical properties of cement-based materials [19,20]. Traditional methods (e.g., TG, SEM, etc.) for the evaluation of the microstructure and properties of cement-based materials yield the destruction of the specimens. However, the EIS technique has the advantages of simplicity, rapidity and nondestructiveness compared with the traditional test methods.

With the development of high-performance concrete, the superplasticizer plays a major role in concrete design. Among which, a polycarboxylate superplasticizer is the most widely used by virtue of its excellent performance. There are many  $\text{Ca}^{2+}$ ,  $\text{Na}^+$ ,  $\text{K}^+$ ,  $\text{OH}^-$  and  $\text{SO}_4^{2-}$  in fresh cement paste, owing to the dissolution of the cement clinker, and the single charged cations ( $\text{K}^+$ ,  $\text{Na}^+$ ) contribute to the direct current conductivity [21–25]. As cement contacts with water,  $\text{Ca}^{2+}$  is introduced in the paste and is adsorbed on the particle surface, resulting in a positive charge on the particle surface. When the superplasticizer is added, polycarboxylic acid, with graft chains, adsorbs on the cement particle surface, hindering cement hydration and reducing the number of  $\text{Ca}^{2+}$  [26]. The carboxyl group on the main chain of the superplasticizer can act as a ligand with  $\text{Ca}^{2+}$  and coordinate with  $\text{Ca}^{2+}$ , and it yields a lower  $\text{Ca}^{2+}$  concentration and reduced conductivity in the cement paste [26,27]. As the cement hydration continues (>3 h), the concentration of  $\text{Ca}^{2+}$  and  $\text{SO}_4^{2-}$  gradually decreases, and the hydroxide ions are the main contributors to the overall conductivity in the cement paste [22–25]. The chloride ions contained in concrete components mainly originate from admixtures such as the early strength agents that are chloride-based. Chloride ions have a positive impact on the mechanical properties and refine the pore structure of cement-based materials [28–30]. When chloride ions are incorporated in cement, they react with the  $\text{C}_3\text{A}$  in cement to form Friedel salts and promote the hydration of  $\text{C}_3\text{A}$ ; meanwhile, they accelerate the hydration of  $\text{C}_3\text{S}$ , consume the  $\text{Ca}(\text{OH})_2$  in the solution, and, thus, affect cement hydration [30–34]. To date, the early hydration properties and electrochemical properties of nano-metakaolin cement paste under the effects of a superplasticizer and chloride ions are not yet clear. Research needs to be carried out.

In this paper, based on EIS technology, the hydration and electrochemical properties of cement paste were investigated within 24 h of contact between cement and water, and the effects of nano-metakaolin, a superplasticizer and chloride ions were considered. To obtain Nyquist plots and Bode plots with impedance modules in EIS, the real part, imaginary part, impedance modulus and frequency values of impedance were obtained. According to Nyquist plots and Bode plots with impedance modules, to calculate the pore solution resistance and impedance modulus, the electrochemical characteristics of the cement paste

were analyzed, and the change in the physical and chemical properties of the cement paste with hydration time was evaluated.

## 2. Experimental Procedures

### 2.1. Materials

Ordinary Portland 42.5 R cement was used in this study. A commercial NMK was manufactured by Inner Mongolia chaopai metakaolin Co., Ltd. (Inner Mongolia, China), and the average flake thickness of NMK was 30 nm. The oxide composition of NMK and cement is shown in Table 1. The main components of NMK were silicon dioxide and alumina. Tap water was utilized in this study. Analytically pure sodium chloride was used in the test. The type of superplasticizer was Polycarboxylate-based which was provided by Shanghai chenqi chemical Co., Ltd. (Shanghai, China), and the water reducing ratio was 25%.

**Table 1.** The chemical composition of NMK and cement.

Chemical Composition (wt%)	SiO <sub>2</sub>	Al <sub>2</sub> O <sub>3</sub>	Fe <sub>2</sub> O <sub>3</sub>	CaO	MgO	SO <sub>3</sub>	K <sub>2</sub> O	Na <sub>2</sub> O	LOI
Cement	21.91	6.27	3.78	59.30	1.64	2.41	-	-	4.69
NMK	49.40	43.88	0.51	0.27	2.66	0.14	0.23	1.52	0.59

### 2.2. Preparation of Cement Pastes

In the test, the water binder (w/b) ratio of the investigated cement paste was 0.4. The replacement level (by mass of cement) of NMK was 1%, and the sample was labelled as NP1. The ordinary cement paste was labelled as NP0. When considering the effects of chloride ions and superplasticizer, the dosages of sodium chloride and superplasticizer were 2% and 0.16%, respectively. To avoid the agglomeration of NMK in the cement paste, NMK firstly went through ultrasonic dispersion for 15 min in water, and then cement was added in the suspension for mixing. As superplasticizer or sodium chloride mixed in the cement paste for preparation, superplasticizer or sodium chloride was firstly added into water for mixing. Next, NMK was incorporated for ultrasonic dispersion after superplasticizer or sodium chloride was fully dissolved in water. After the paste preparation was completed, it was cast in a 40 mm × 40 mm × 40 mm plastic mold, and a pair of stainless-steel plate electrodes (39.6 mm × 60 mm × 0.5 mm) were inserted in the opposite direction inside the mold.

### 2.3. Testing Method

Bio Logic SP300 electrochemical workstation was selected for EIS test. In the electrochemical impedance spectroscopy test, the frequency affected the experimental results. For low-frequency testing, the lower the set frequency, the more complete an electrochemical impedance spectrum could be obtained, but the longer the testing time. Due to the rapid development of the structural buildup of cement-based materials in the early hydration stage, a great deviation to the EIS measurement was caused. Therefore, a longer testing time was not conducive to the experiment of the electrochemical impedance of cement-based materials at initial stages. In this paper, the electrochemical impedance test frequency range was 7 MHz to 0.01 Hz, the voltage amplitude was 10 mV, and 10 test points were selected for each frequency range. Then, the two-probe method was chosen for electrochemical impedance spectrum testing.

## 3. Results and Discussion

### 3.1. EIS of Ordinary Cement Paste

Nyquist plots of the cement paste consist of high-frequency and low-frequency regions corresponding to the bulk material effect and the polarization effect of the electrode/specimen [17,18]. Figure 1 shows the Nyquist plots of ordinary cement paste at the hydration time of 15 min to 2 h. The horizontal coordinate  $Z'$  is the real part of

the impedance in Nyquist plots. The vertical coordinate  $Z''$  is the imaginary part of the impedance. It can be seen that there was no capacitive arc in the region of high frequency of the Nyquist plots (the left part); moreover, the Nyquist plots presented a negative capacitance before the 12 h after cement contacted with water. The rate and number of positive and negative ions moving in the solution produced a limited current signal lagging behind the rate of change of the high-frequency alternating current. This resulted in the inability to transfer electrons properly, and only charge transfers occurred. The movement of directional dipoles on the electrode surface could not keep up with the changes in the electric field, thus, yielding a blocking effect which was expressed as a negative capacitance [34]. Electrochemical reactions could only take place at the surface of hydration products (e.g., C-S-H gels, etc.); therefore, electrochemical reactions could only take place properly when there were sufficient hydration products, such as C-S-H gels, existing in the cement paste [34,35]. At this stage, the interior of the cement paste was mostly pore solution, and sufficient C-S-H gels had not yet appeared. Additionally, there was not a reliable electrochemical reaction interface inside the cement paste. The intersection of the high-frequency region with the horizontal axis of  $Z'' = 0$  was the pore solution resistance  $R_s$ . The pore solution resistance was the resistance of the electrolytes in the solution. The higher the concentration of ions in the pore solution and the greater the porosity, the lower the pore solution resistance. The pore solution resistances of ordinary cement paste hydrated for 15 min, 2 h, 4 h, 8 h and 12 h were 19.1  $\Omega$ , 17.6  $\Omega$ , 18.3  $\Omega$ , 20.8  $\Omega$  and 25.2  $\Omega$ , respectively. The pore solution resistance first decreased and then increased with hydration time. This was caused by the contact between cement and water, and the cement clinker and a variety of ions, including anions ( $\text{SO}_4^{2-}$ ,  $\text{OH}^-$ ) and cations ( $\text{Ca}^{2+}$ ,  $\text{Na}^+$ ,  $\text{K}^+$ ), dissolved in the pore solution. The presence of charged ions led to a decrease in the pore solution resistance of the cement paste, and this stage was primarily determined by the initial dissolution behavior of the cement clinker [16,36]. As the cement hydration reaction proceeded, the ions that dissolved in the paste increased rapidly and reached saturation in a short time. Furthermore, the stage was primarily controlled by cement hydration, although the degree of cement hydration was weaker during the acceleration period [16,36]. When the ion concentration reached the critical nucleation concentration, the stable hydrate phases began to nucleate, and the ion concentration then decreased [37]. The  $R_s$  in the cement paste depended mainly on the ion concentration in the pore solution, and the ion concentration in the pore solution gradually decreased as the hydration time increased. The C-S-H gels and solids produced by hydration clogged the pore structure, yielding a decrease in porosity [35]. When the cement contacted with water for 24 h, the negative capacitance of the high-frequency region of the impedance spectrum of ordinary cement paste disappeared. The capacitive arc started to appear in the high-frequency region, and the formation of the capacitive arc indicated that the disconnected pore structure inside the cement paste had begun to form [19].

The impedance modulus  $|Z|$  signifies the hinder effect for the current conduction in the cement paste. Bode plots with the impedance modules of ordinary cement paste are presented in Figure 2. It can be seen that with the hydration of cement, the impedance modules  $|Z|$  of ordinary cement paste first decreased and then increased. When the applied frequency was 0.01 Hz, the cement paste impedance modules were 37.9 k $\Omega$ , 41.7 k $\Omega$ , 44.3 k $\Omega$ , 46.9 k $\Omega$ , 49.5 k $\Omega$  and 51.2 k $\Omega$  at 15 min, 2 h, 4 h, 8 h, 12 h and 24 h of hydration, respectively. Furthermore, the impedance modules of the cement paste produced a larger response to the interference frequency at a lower frequency. When the applied frequency was 7 MHz, the cement paste impedance moduli were 15.8  $\Omega$ , 14.8  $\Omega$ , 15.2  $\Omega$ , 16.9  $\Omega$ , 20.1  $\Omega$  and 47.0  $\Omega$  for cement hydration up to 15 min, 2 h, 4 h, 8 h, 12 h and 24 h, respectively. The decrease of the impedance modules for cement hydration from 15 min to 2 h was also related to the dissolution of the cement clinker. The impedance modules varied more in the region where the high and low frequencies intersected (the intersection of the semicircle and the straight line in the Nyquist plots). The trend of variation also represented the limit of capacitance and may be linked to the microstructure

of the cement paste and the pore fillings. When the hydration products in the cement paste gradually filled the pore structure, channels inside the pore structure were formed, the ion migration rate was accelerated, and the material transfer rate increased. The resistance of the cement paste continuously decreased, which was expressed in the Bode plots with impedance modules as an increase in the slope of the decline. Thus, the higher the degree of hydration and the more pore fillers (hydration products), the smaller the average pore size inside the paste, and the narrower the interconnected paths in the capillaries [38]. Along with the cement hydration, the rate of decrease of the curve in the Bode plots with impedance modules increased, and the capacitance limit increased. In a word, the higher the degree of cement hydration and the more pore fillers (hydration products) there were.

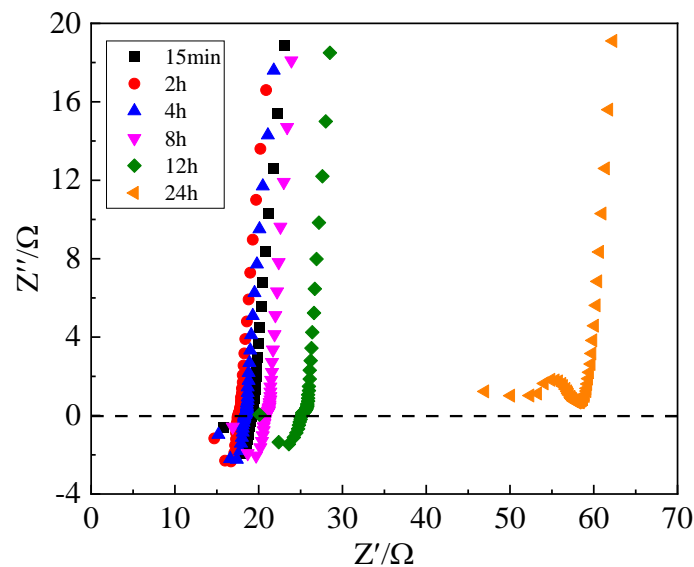


Figure 1. Nyquist plots of ordinary cement paste.

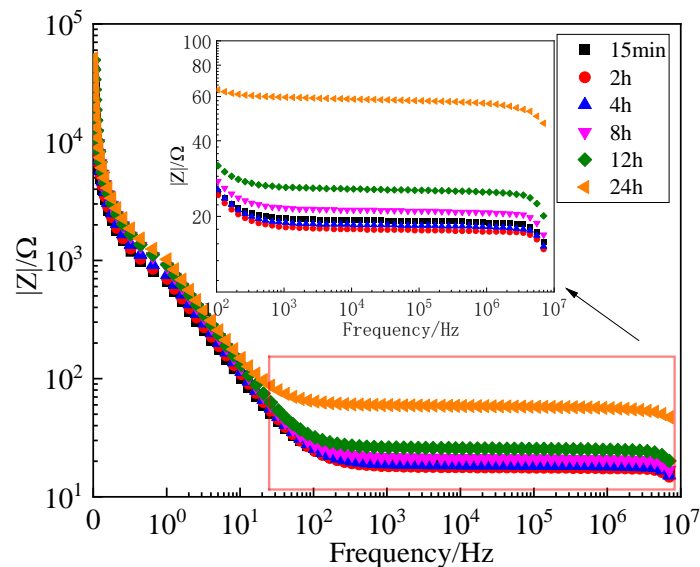
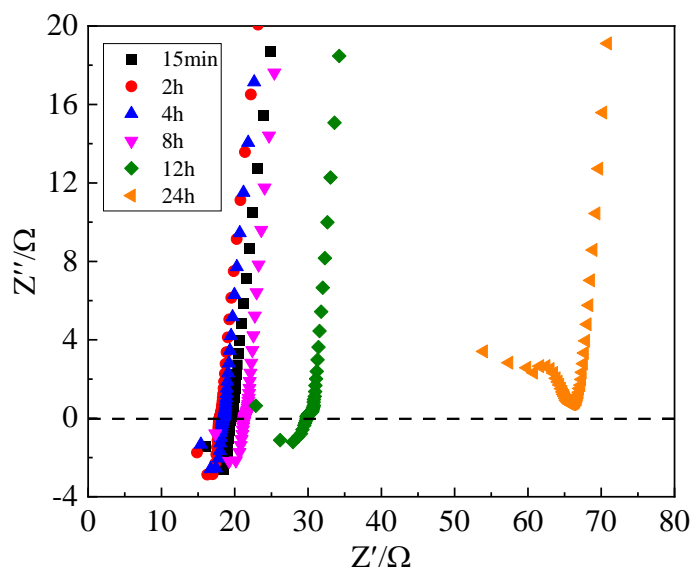


Figure 2. Bode plots with impedance modules of ordinary cement paste.

### 3.2. EIS of NMK Cement Paste

Nyquist plots of the cement paste with 1% NMK are shown in Figure 3. It can be seen that the Nyquist plots of 1% nano-metakaolin cement paste were similar to that of ordinary cement paste during 15 min to 12 h of hydration. The high-frequency region of the electrochemical impedance spectrum also showed negative capacitance and no capacitive arc. Here, the internal structure of NP1 cement paste had not yet built up, the

internal structure of cement paste had not yet been filled with sufficient C-S-H gel, and the paste was filled with the pore solution. The hindrance effect kept the internal charge of the cement paste from being transferred normally, and there no electrochemical reaction occurred. This finally led to the partial-negative capacitance in the high-frequency region of the impedance spectrum of ordinary cement paste. Similarly, when cement hydration came to 24 h, the negative capacitance in the high-frequency region of the impedance spectrum of NP1 cement paste disappeared. At this time, a large number of microscopic pore structures inside the cement paste had been initially filled with hydration products such as C-S-H gels, and the electrochemical reactions began to proceed normally. At this point, the appearance of the capacitive resistance arc in the high-frequency region indicated that the disconnected micropore channel structure inside the NMK cement paste started to form gradually. When the hydration time came to 15 min, 2 h, 4 h, 8 h and 12 h, the pore solution resistances of NP1 cement paste were 19.4  $\Omega$ , 17.9  $\Omega$ , 18.4  $\Omega$ , 21.4  $\Omega$  and 29.8  $\Omega$ , respectively. Additionally, the pore solution resistance at every age was greater than that of ordinary cement paste. With the development of cement hydration, the growth rate of pore solution resistance of NP1 cement paste was slightly faster than that of the ordinary cement. The negative capacitance arc in the high-frequency region of the Nyquist plots of NP1 paste were reduced compared with that of ordinary cement paste. Furthermore, NP1 cement paste had more hydration products, and the structural build-up rate was faster than that of NP0 cement paste. On the one hand, the SiO<sub>2</sub> content was highest in NMK, and the Al<sub>2</sub>O<sub>3</sub> content was the second highest, which were favorable for the promotion of cement hydration and the reduction of the setting time [39]. On the other hand, this was caused by the small particle size of NMK particles, and NMK provided more nucleation sites offered and promoted cement hydration, accelerating the formation of hydration products in the cement paste [40,41]. With the progress of cement hydration, the residual insoluble solid hydration products in the cement paste precipitated and then sedimented, overlapped and accumulated with each other to form a structural skeleton [16]. Furthermore, the addition of NMK to the cement paste increased the viscosity of the fresh cement paste [42], which decreased the rate of ion migration in the cement paste.



**Figure 3.** The Nyquist plots of cement paste with 1% NMK addition.

As can be seen from Figure 4, the Bode plots with impedance modules of NP1 cement paste followed the same pattern of variation as that of ordinary cement paste. When the applied frequency was low (0.01 Hz), the NP1 cement paste impedance had a larger response to the disturbance. At the hydration times of 15 min, 2 h, 4 h, 8 h, 12 h and 24 h, the NP1 cement paste impedance moduli were 27.8 k $\Omega$ , 31.6 k $\Omega$ , 32.9 k $\Omega$ , 35.9 k $\Omega$ , 39.0 k $\Omega$  and 42.7 k $\Omega$ , respectively. When the applied frequency was 7 MHz, the impedance moduli

of the cement paste at 15 min, 2 h, 4 h, 8 h, 12 h and 24 h were 16.1  $\Omega$ , 15.0  $\Omega$ , 15.4  $\Omega$ , 17.4  $\Omega$ , 22.9  $\Omega$  and 54.1  $\Omega$ , respectively. This phenomenon also indicated that NP1 cement paste hydrates faster and has more hydration products in the same hydration period. Nanoparticles filled the voids between larger cementitious particles and yielded a denser packing of cementitious particles at the nanoscale. Moreover, nanoparticles provided a seeding surface for hydrate deposition and promoted cement hydration, accelerating the formation of hydration production [37]. The denser packing and the hydration products promoted the formation of internal structural buildup, and the channels for ion transports were blocked over time. Therefore, the hinder effect for the current conduction in the cement paste increased with NMK addition, and the impedance modules increased.

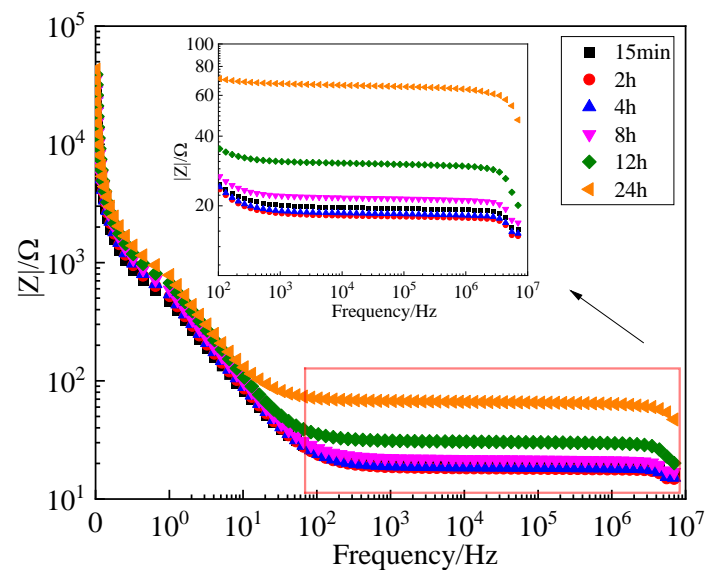


**Figure 4.** The Bode plots with impedance modules of cement paste with 1% NMK addition.

### 3.3. EIS of Cement Paste with the Addition of Superplasticizer

Nyquist plots of ordinary cement paste and 1% NMK cement paste with the superplasticizer are shown in Figure 5. As the superplasticizer was added, the ordinary cement paste and the cement paste with 1% NMK addition were labelled as SP-NP0 and SP-NP1, respectively. Keeping Figure 5 in mind, the Nyquist curve showed negative capacitance in the high-frequency region, and the pore solution resistance first decreased and then increased along with cement hydration. The pore solution resistances at 15 min, 2 h, 4 h, 8 h and 12 h of SP-NP0 cement paste were 17.0  $\Omega$ , 16.6  $\Omega$ , 15.6  $\Omega$ , 17.7  $\Omega$  and 20.3  $\Omega$ , respectively. The variation of pore solution resistance characterized the hydration process of cement. Within a short time of contact between cement and water, the solid particles were homogeneously dispersed in the solution, there were more solid particles in the unit volume, and the pore solution resistance was larger. With the dissolution of the cement clinker, the ion concentration in the solution increased, and the pore solution resistance decreased. With the development of hydration, solid particles in the cement paste gradually accumulated, and hydration products gradually filled the inter-particle voids. At that moment, the solution existed between the solid-particle voids, with the structural buildup and the accumulation of hydration products over time, the ion transport channels narrowing down, and the pore solution resistance continuing to grow. Compared with the NP0 cement paste, the pore solution resistance of SP-NP0 was small. The reason for this was that, on the one hand, the superplasticizer had the role of electrostatic repulsion and steric hindrance after being added into the cement paste, dispersing the flocculation structures, releasing flocculated water, reducing the viscosity of the cement paste [42] and accelerating the rate of ion transport. On the other hand, excess anions in the superplasticizer were dispersed in the cement paste; the ion concentration in the paste increased, and the pore solution resistance decreased.

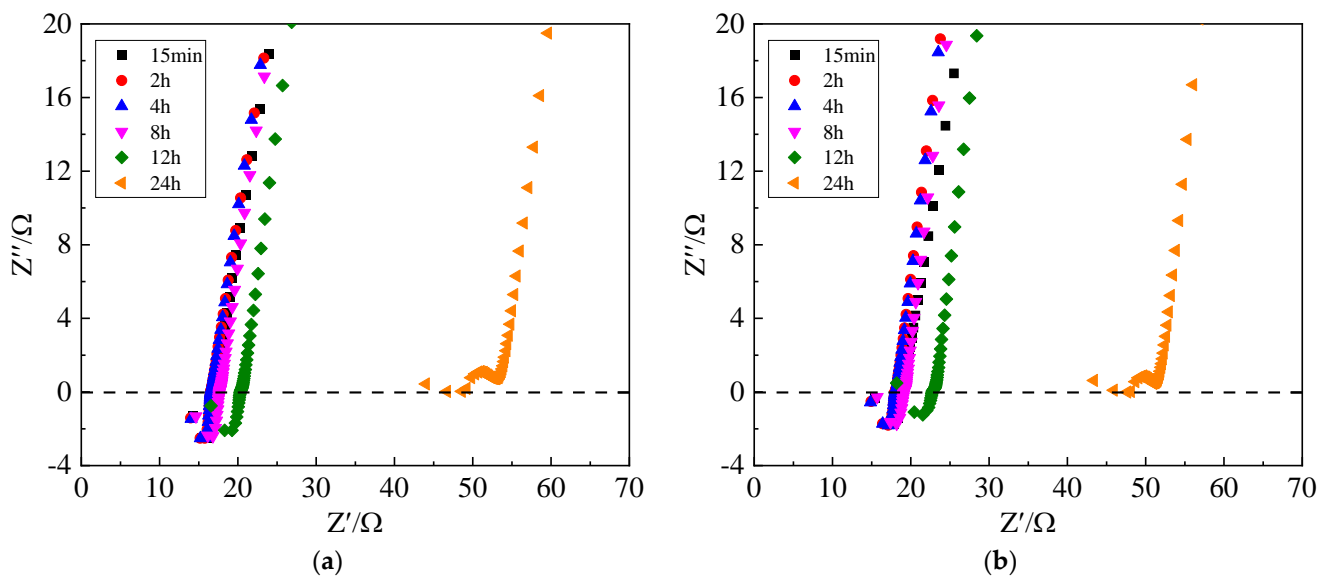


**Figure 5.** The Nyquist plots of cement paste with superplasticizer. (a) SP-NP0; (b) SP-NP1.

Compared with SP-NP0, the pore solution resistance of SP-NP1 cement paste increased. When the cement paste hydrated for 15 min, 2 h, 4 h, 8 h, and 12 h, the pore solution resistances of SP-NP1 were 18.9  $\Omega$ , 17.9  $\Omega$ , 18.0  $\Omega$ , 19.2  $\Omega$ , and 22.8  $\Omega$ , respectively. Wang et al. [43] believed that nanoclay particles adsorb more strongly on the superplasticizer than on the cement particles. Therefore, the number of excess anions of the superplasticizer in NMK cement paste decreased, and the pore solution resistance increased. When the cement hydrated for 24 h, the negative capacitance disappeared completely and gradually formed the capacitive resistance arc. The Bode plots with the impedance modules of SP-NP0 and SP-NP1 cement paste are shown in Figure 6. As the cement hydrated for 15 min, 2 h, 4 h, 8 h and 12 h, the impedance moduli of SP-NP0 cement paste at the applied frequency of 0.01 Hz were 41.1 k $\Omega$ , 45.12 k $\Omega$ , 46.4 k $\Omega$ , 47.6 k $\Omega$  and 47.7 k $\Omega$ , respectively. Additionally, at the applied frequency of 7 MHz, the impedance moduli of the paste were 17.5  $\Omega$ , 15.3  $\Omega$ , 15.4  $\Omega$ , 16.3  $\Omega$  and 18.4  $\Omega$ , respectively. For SP-NP1 cement paste at the applied frequency of 0.01 Hz, the impedance moduli were 34.1 k $\Omega$ , 38.5 k $\Omega$ , 40.3 k $\Omega$ , 44.4 k $\Omega$  and 47.6 k $\Omega$ , respectively. Furthermore, at the applied frequency of 7 MHz, the impedance moduli were 17.2  $\Omega$ , 16.4  $\Omega$ , 16.5  $\Omega$ , 17.5  $\Omega$  and 20.4  $\Omega$ , respectively. The impedance modulus characterized the impedance of the cement paste to the current, which increased with hydration time from 2 h to 24 h, and the impedance modulus of the paste increased gradually with the internal structural buildup of fresh cement paste.

### 3.4. EIS of Cement Paste with the Addition of Chloride Ions

The Nyquist plots of ordinary cement paste and 1% NMK cement paste with chloride ions are shown in Figure 7. As sodium chloride was added, the ordinary cement paste and the cement paste with 1% NMK addition were labelled as Cl-NP0 and Cl-NP1, respectively. In Figure 7, it can be seen that the Nyquist plots of the cement paste with chloride ions changed. The curves were straight lines until 8 h of cement hydration. The Nyquist plots of Cl-NP0 cement paste showed no capacitive arc at 24 h. The Nyquist plots of Cl-NP1 cement paste were basically the same as those of Cl-NP0 cement paste before 12 h of contact between cement and water. When the cement hydrated to 24 h, the Nyquist plots of Cl-NP1 cement paste showed an obvious resistance capacitive arc, indicating that sufficient C-S-H gels had accumulated inside the paste and that the electrochemical reactions inside the paste proceeded normally. The pore solution resistances at 15 min, 2 h, 4 h, 8 h and 12 h of Cl-NP0 cement paste were 7.8  $\Omega$ , 7.5  $\Omega$ , 7.68  $\Omega$ , 8.8  $\Omega$  and 13.0  $\Omega$ , respectively. For the Cl-NP1 cement paste, when cement paste hydrated for 15 min, 2 h, 4 h, 8 h, and 12 h, the

pore solution resistances of SP-NP1 were 7.9  $\Omega$ , 7.9  $\Omega$ , 8.0  $\Omega$ , 9.2  $\Omega$  and 13.9  $\Omega$ , respectively. This was due to the fact that sodium chloride is a strong soluble electrolyte, completely electrolyzed in water to  $\text{Na}^+$  and  $\text{Cl}^-$ . Sodium chloride was added into the cement paste, the ion concentration in the paste increased, and the pore solution resistance of the cement paste with chloride ions decreased.

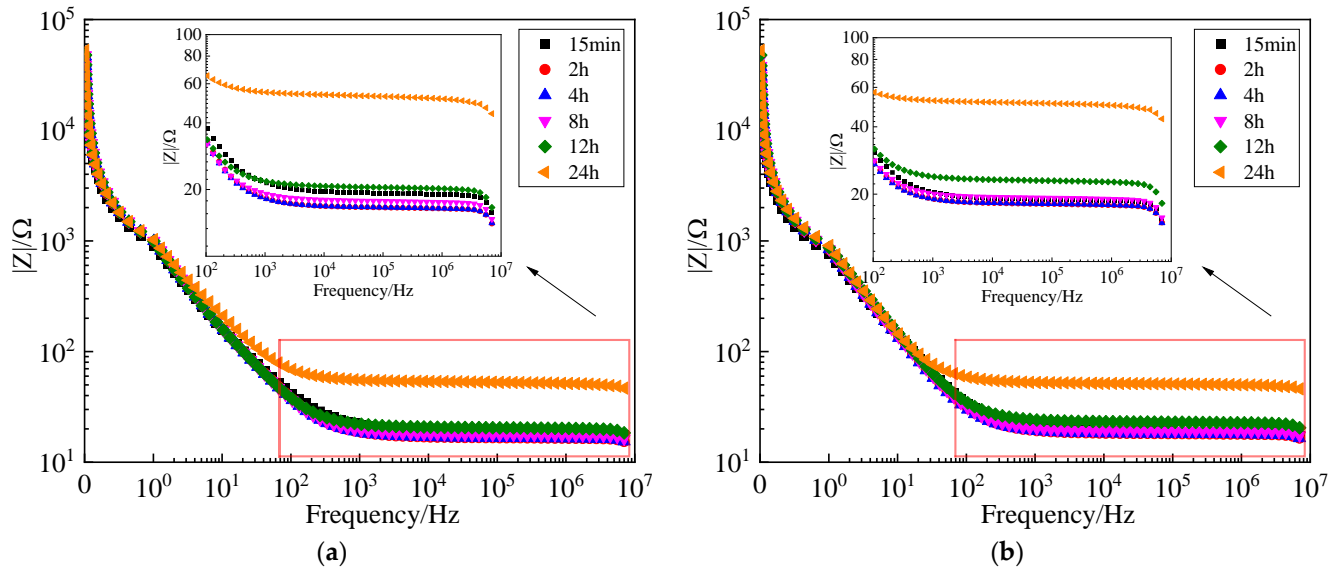


**Figure 6.** Bode plots with impedance modules of cement paste with superplasticizer addition. (a) SP-NP0; (b) SP-NP1.

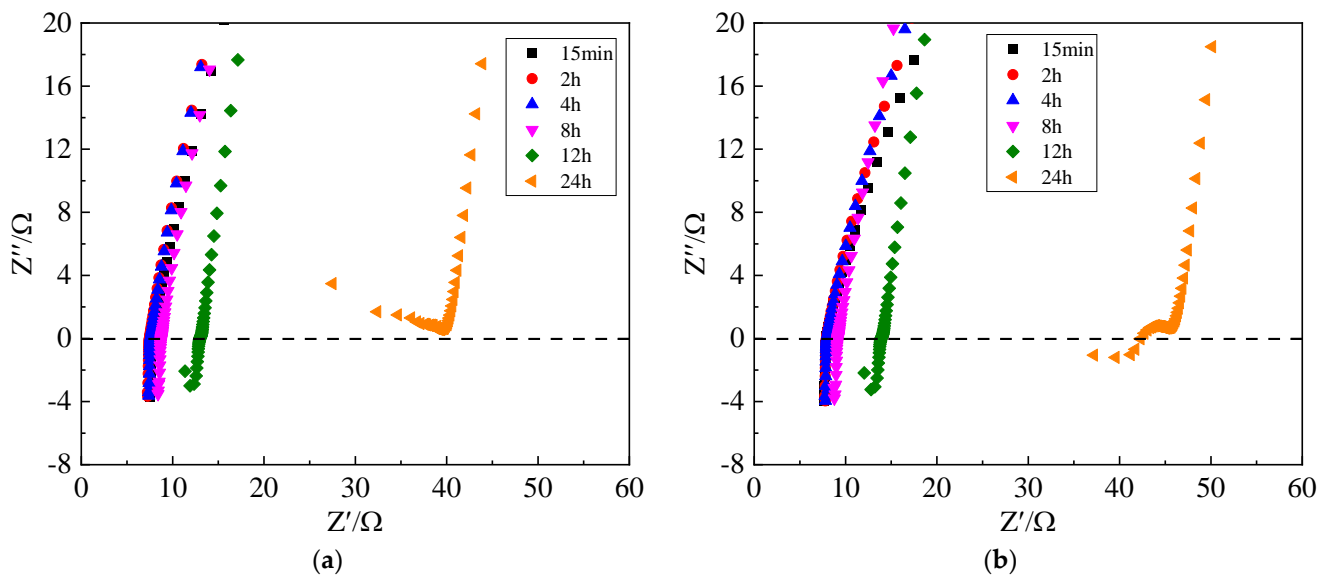


**Figure 7.** The Nyquist plots of cement paste with sodium chloride. (a) Cl-NP0; (b) Cl-NP1.

The Bode plots with impedance modules of Cl-NP0 and Cl-NP1 cement pastes are shown in Figure 8. According to Figure 8, as the cement hydrated for 15 min, 2 h, 4 h, 8 h, 12 h and 24 h, the impedance moduli of Cl-NP0 cement paste at 0.01 Hz were 40.4 k $\Omega$ , 44.8 k $\Omega$ , 46.2 k $\Omega$ , 46.5 k $\Omega$ , 46.7 k $\Omega$  and 47.6 k $\Omega$ , respectively. And at 7 MHz, the impedance moduli of the paste were 8.4  $\Omega$ , 8.1  $\Omega$ , 8.2  $\Omega$ , 9.0  $\Omega$ , 11.6  $\Omega$  and 27.7  $\Omega$ , respectively. For Cl-NP1 cement paste at 0.01 Hz, the impedance moduli were 41.4 k $\Omega$ , 46.2 k $\Omega$ , 48.0 k $\Omega$ , 47.6 k $\Omega$ , 48.4 k $\Omega$  and 49.0 k $\Omega$ , respectively. While the applied frequency was 7 MHz, the impedance moduli were 8.6  $\Omega$ , 8.5  $\Omega$ , 8.7  $\Omega$ , 9.3  $\Omega$ , 12.2  $\Omega$  and 37.2  $\Omega$ , respectively. During the 12 h of cement-water contact, the variation of the pore solution resistance and the impedance modulus at the high-frequency response of the cement paste with chloride

ion addition was small compared to the cement paste without sodium chloride. It was demonstrated that chloride ions promoted the dissolution of gypsum in the cement paste, and they accelerated the formation of calcium alumina, which accelerated cement hydration by promoting crystalline nucleation and crystal growth during cement hydration [30,32]. Meanwhile, sodium chloride and  $\text{Ca}(\text{OH})_2$  crystals generated chloride ions and calcium ions through the salt effect in fresh cement paste, which in turn reacted with  $\text{C}_3\text{A}$  to form Friedel salt ( $\text{C}_3\text{A}\cdot\text{CaCl}_2\cdot 10\text{H}_2\text{O}$ ) (Equation (1)). Furthermore, the Friedel salt that was generated bound to a part of  $\text{Na}^+$ , thus reducing the concentration of free chloride ions and sodium ions in the solution [13,15].

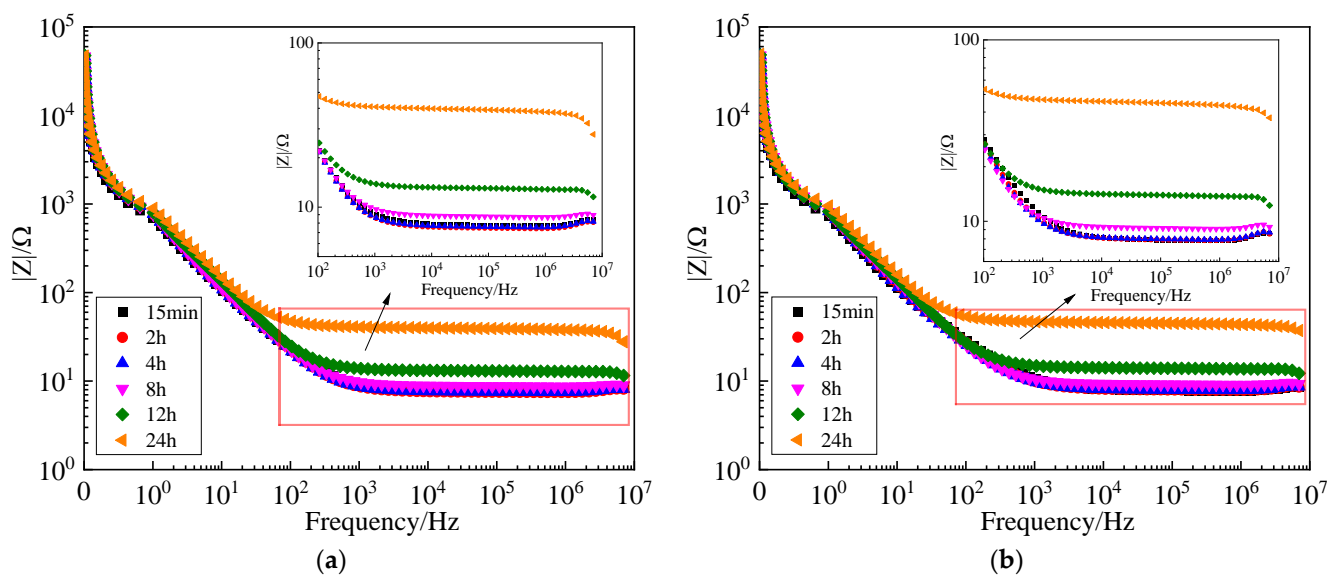


**Figure 8.** Bode plots with impedance modules of cement paste with superplasticizer addition. (a) CI-NP0; (b) CI-NP1.

Previous studies have clearly shown that, in the incorporation of sodium chloride into the cement paste, Friedel salt is not generated in the early stage of hydration [30]. Additionally, only as a calcium alumina becomes a monosulfide type calcium alumina,  $\text{Cl}^-$  starts to react to form Friedel salt, and the  $\text{Cl}^-$  concentration decreases after 10 h of hydration [30,32]. Compared to hydration for 8 h, the pore solution resistances of CI-NP0 and CI-NP1 cement pastes hydrated for 12 h increased by 66.7% and 76.0%, respectively. The growth rate of the CI-NP1 pore solution resistance of the cement paste was faster due to the promotion of NMK particles in cement hydration. It indicated that the nano-metakaolin still has a positive effect on the hydration of the cement paste with the chloride ion addition.

#### 4. The Variation of Pore Solution Resistance and Impedance Modulus

The effect of the addition or non-addition of the superplasticizer/sodium chloride on the pore solution resistance and impedance modulus of ordinary cement paste and the paste with 1% NMK addition is illustrated in Figure 9. The pore solution resistance, i.e., the charge transfer resistance, was inversely proportional to the porosity and ion concentration in the cement paste. From Figure 9a, it can be seen that for a certain content of the superplasticizer or sodium chloride, the solution resistance of the cement paste with 1% NMK addition was always greater than the solution resistance of ordinary cement paste, which was attributed to the filler and nucleation effects of NMK in the cement paste, the porosity of the paste, the promotion of cement hydration, and the acceleration of the generation of hydration products, which yielded an increase in the pore solution resistance of the cement paste. The  $\text{SiO}_2$  content was the highest in NMK, and the  $\text{Al}_2\text{O}_3$  content was the second highest, which were favorable for the promotion of cement hydration and the

reduction of the setting time [39]. The nucleation effect of the nanoclay promoted C-S-H precipitation, and the pozzolanic activity consumed  $\text{Ca}(\text{OH})_2$ . Additionally, the reduction of free calcium ions in the early stage of cement hydration stimulated the dissolution of cement particles, accelerating the hydration rate of  $\text{C}_3\text{S}$  and shortening the dormant period [44,45]. Submicron/nanoclay had little effect on the hydration heat within about 8 h, and when the cement contacted with water for about 8–24 h, the exothermic peak of the hydration heat curve increased with the increase of submicron/nanoclay content [44–46]. It can be seen from Figure 9 that when the cement contacted with water within about 8 h, the pore solution resistance and impedance modulus were less affected by NMK. When the cement hydration was over about 8 h, the pore solution resistance and impedance modulus of the cement paste were significantly improved by the addition of 1% NMK. The pore solution resistances of the cement paste with 1% NMK were increased by 0.49%, 2.64% and 18.17% as compared with ordinary cement paste when the hydration time was 4 h, 8 h and 12 h, respectively. When the cement was in contact with water for 4 h, the pore solution resistances of NP1, SP-NP1 and CI-NP1 cement pastes increased by 4.96%, 8.81% and 4.91%, respectively, compared with that of NP0, SP-NP1 and CI-NP1 cement pastes.

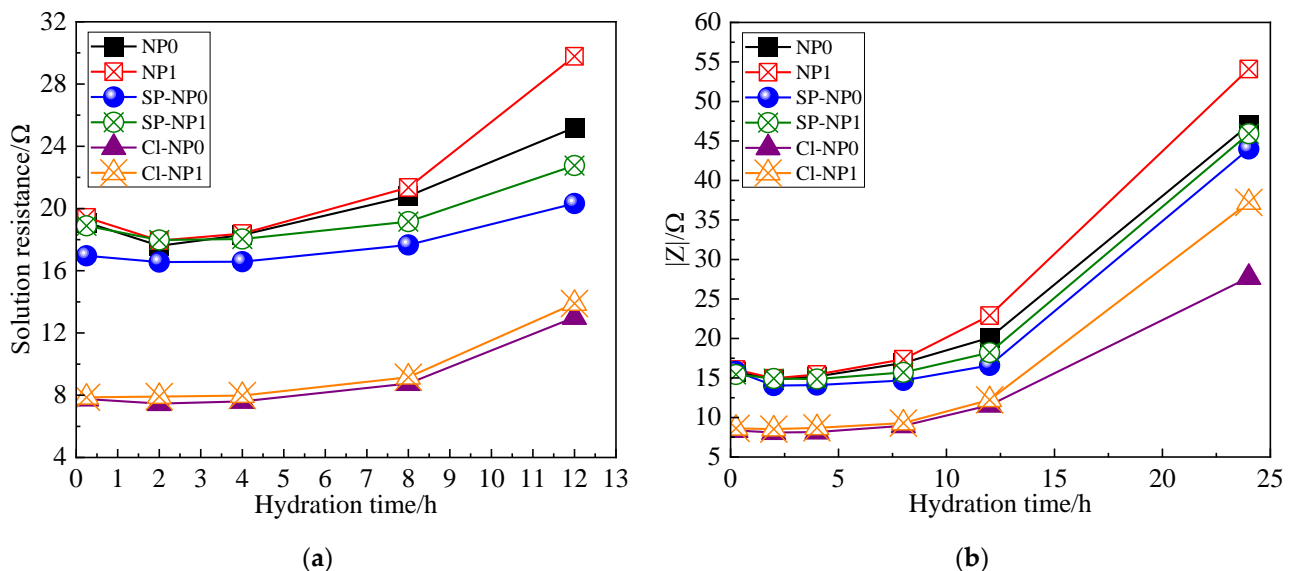


**Figure 9.** The variations of pore solution resistance and impedance modulus in cement paste. (a) Pore solution resistance (b) Impedance modulus.

Compared with the cement paste with the addition of sodium chloride, NMK had the most significant increase in pore solution resistance on the cement paste with the superplasticizer. This was attributed to the adsorption of the superplasticizer on nanoclay particles, which adsorbed more strongly on the superplasticizer than on the cement particles [43]. The enhancement effect of NMK on the pore solution resistance of the cement paste was less affected by chloride ions, and 1% NMK created no significant increase in the solution resistance in the cement paste with chloride ions. For a certain NMK content, both the superplasticizer and sodium chloride caused the reduction of pore solution resistance of the cement paste. Additionally, the reduction of the solution resistance by chloride ions was more significant because the ion concentration in the cement paste was increased more significantly by sodium chloride, so the reduction of the solution resistance of the cement paste by sodium chloride was more obvious. It can also be seen from Figure 9a that the variation in pore solution resistance of the cement paste with the superplasticizer was small within 8 h of contact between cement and water. The reason for this is that after the superplasticizer was added, the superplasticizer molecules adsorbed on the surface of the cement particles, wrapping the cement particles and delaying the hydration of cement, so the variation of the solution resistance was small. Combined with the impedance modulus of the cement paste (Figures 2, 4, 6 and 8), this was found to be the most significant dif-

ference in the high-frequency region, so the impedance modulus of the cement paste at a frequency of 7 MHz was plotted in Figure 9b. It can be seen that the impedance modulus of the cement paste was consistent with the change in pore solution resistance. The impedance modulus of the cement paste decreased first and then increased with the hydration time. The decrease of the impedance modulus in the early stage was attributed to the dissolution of the cement clinker. Along with cement hydration, the internal structure of the cement paste buildup and the microstructure were more dense, and the impedance of the current conduction was enhanced.

## 5. Conclusions

This work investigated the early-age properties and electrochemical properties of NMK cement pastes, and the effects of the superplasticizer and sodium chloride were considered. The variations of pore solution resistance and the impedance modulus with the hydration time in NMK cement paste were discussed. The following conclusions can be drawn:

(1) The solution resistance and impedance modulus of the cement paste decreased first and then increased within 15 min–2 h of cement contact with water. The decrease in pore solution resistance before 2 h was related to the dissolution of the cement clinker, which led to an increase in ion concentration in the paste.

(2) NMK promoted an increase in the pore solution resistance and impedance modulus in the cement paste (hydration for 15 min–12 h) with or without the superplasticizer and sodium chloride. Due to the filler effect, the nucleation effect and pozzolanic activity of NMK, which accelerated the internal structural buildup, yielded the increase of the solution resistance.

(3) The superplasticizer reduced the pore solution resistance and impedance modulus of the cement paste with or without NMK. The superplasticizer dispersed the flocculation structures, released flocculated water, reduced the viscosity of the cement paste and accelerated the rate of ion transport, and the excess anions in the superplasticizer were dispersed in the cement paste. The ion concentration in the cement paste increased, and the pore solution resistance decreased.

(4) Sodium chloride decreased the pore solution resistance and impedance modulus of the cement paste with or without NMK. Sodium chloride was completely electrolyzed in water to  $\text{Na}^+$  and  $\text{Cl}^-$ , the ion concentration in the paste increased, and the pore solution resistance of the cement paste with chloride ions decreased.

**Author Contributions:** Writing—original draft preparation, Q.L.; data curation, Q.L.; formal analysis, Q.L.; resources, Y.F.; writing—review and editing, Y.F.; experiments, Y.Z.; experiments, Z.L. All authors have read and agreed to the published version of the manuscript.

**Funding:** This research was financially supported by the National Natural Science Foundation of China (Grant No. 51578099) to which the authors are very grateful.

**Data Availability Statement:** Data will be made available on request.

**Conflicts of Interest:** The authors declare that they have no known competing financial interest or personal relationship that could have appeared to influence the work reported in this paper.

## References

1. Ramezani, M.; Kim, Y.H.; Sun, Z.; Sherif, M.M. Influence of carbon nanotubes on properties of cement mortars subjected to alkali-silica reaction. *Cem. Concr. Compos.* **2022**, *131*, 104596. [[CrossRef](#)]
2. He, X.; Shi, X. Chloride permeability and microstructure of Portland cement mortars incorporating nanomaterials. *Transp. Res. Rec.* **2008**, *2070*, 13–21. [[CrossRef](#)]
3. Ramezani, M.; Dehghani, A.; Sherif, M.M. Carbon nanotube reinforced cementitious composites: A comprehensive review. *Constr. Build. Mater.* **2022**, *315*, 125100. [[CrossRef](#)]
4. Fan, Y.F.; Zhang, S.Y.; Wang, Q.; Shah, S.P. The effects of nano-calcined kaolinite clay on cement mortar exposed to acid deposits. *Constr. Build. Mater.* **2016**, *102*, 486–495. [[CrossRef](#)]

5. Madandoust, R.; Mousavi, S.Y. Fresh and hardened properties of self-compacting concrete containing metakaolin. *Constr. Build. Mater.* **2012**, *35*, 752–760. [[CrossRef](#)]
6. Abo-El-Enein, S.A.; Amin, M.S.; El-Hosiny, F.I.; Hanafi, S.; ElSokkary, T.M.; Hazem, M.M. Pozzolanic and hydraulic activity of nano-metakaolin. *HBRC J.* **2014**, *10*, 64–72. [[CrossRef](#)]
7. Morsy, M.S.; Shoukry, H.; Mokhtar, M.M.; Ali, A.M.; El-Khodary, S.A. Facile production of nano-scale metakaolin: An investigation into its effect on compressive strength, pore structure and microstructural characteristics of mortar. *Constr. Build. Mater.* **2018**, *172*, 243–250. [[CrossRef](#)]
8. Shoukry, H.; Kotkata, M.F.; Abo-el-Enein, S.A.; Morsy, M. Flexural strength and physical properties of fiber reinforced nano metakaolin cementitious surface compound. *Constr. Build. Mater.* **2013**, *43*, 453–460. [[CrossRef](#)]
9. Fan, Y.F.; Zhang, S.Y.; Kawashima, S.; Shah, S.P. Influence of kaolinite clay on the chloride diffusion property of cement-based materials. *Cem. Concr. Compos.* **2014**, *45*, 117–124. [[CrossRef](#)]
10. Quanji, Z.; Lomboy, G.R.; Wang, K. Influence of nano-sized highly purified magnesium alumino silicate clay on thixotropic behavior of fresh cement pastes. *Constr. Build. Mater.* **2014**, *69*, 295–300. [[CrossRef](#)]
11. Muhd, N.M.S.; Hamidah, M.S.; Mohd, F.A.; Bao, Y.; Guo, P.; Lyu, Z.; Abu-obeidah, A.; Nassif, H.; Wang, H. Inclusion of nano metakaolin as additive in ultra high performance concrete (UHPC). *Constr. Build. Mater.* **2016**, *127*, 167–175. [[CrossRef](#)]
12. Dong, B.Q.; Gu, Z.T.; Qiu, Q.W.; Li, X.; Bai, X.; He, B.; Niu, S.; Sun, F. Electrochemical feature for chloride ion transportation in fly ash blended cementitious materials. *Constr. Build. Mater.* **2018**, *161*, 577–586. [[CrossRef](#)]
13. Shi, M.; Chen, Z.; Sun, J. Determination of chloride diffusivity in concrete by AC impedance spectroscopy. *Cem. Concr. Res.* **1999**, *29*, 1111–1115. [[CrossRef](#)]
14. Etteyeb, N.; Dhoubi, L.; Takenouti, H.; Triki, E. Protection of reinforcement steel corrosion by phenylphosphonic acid pre-treatment PART II: Tests in mortar medium. *Cem. Concr. Compos.* **2016**, *65*, 94–100. [[CrossRef](#)]
15. Keddam, M.; Takenouti, H. Impedance measurements on cement paste. *Cem. Concr. Res.* **1997**, *27*, 1191–1201. [[CrossRef](#)]
16. Cai, R.J.; He, Z.; Tang, S.W.; Wu, T.; Chen, E. The early hydration of metakaolin blended cements by non-contact impedance measurement. *Cem. Concr. Compos.* **2018**, *92*, 70–81. [[CrossRef](#)]
17. Huang, T.J.; Yuan, Q.; Zuo, S.H.; Li, B.; Wu, Q.; Xie, Y. Evaluation of microstructural changes in fresh cement paste using AC impedance spectroscopy vs. oscillation rheology and <sup>1</sup>H NMR relaxometry. *Cem. Concr. Res.* **2021**, *149*, 106556. [[CrossRef](#)]
18. Hu, X.; Shi, C.J.; Liu, X.J.; Zhang, J.; de Schutter, G. A review on microstructural characterization of cement-based materials by AC impedance spectroscopy. *Cem. Concr. Compos.* **2019**, *100*, 1–14. [[CrossRef](#)]
19. Song, G.L. Equivalent circuit model for AC electrochemical impedance spectroscopy of concrete. *Cem. Concr. Res.* **2000**, *30*, 1723–1730. [[CrossRef](#)]
20. Dong, B.; Li, G.; Zhang, J.; Liu, Y.; Xing, F.; Hong, S. Non-destructive tracing on hydration feature of slag blended cement with electrochemical method. *Constr. Build. Mater.* **2017**, *149*, 467–473. [[CrossRef](#)]
21. Huang, W.; Zhou, J.M.; Zhong, C.H.; Ma, X.X.; Fang, Y.H.; Ke, Y.L.; Wei, J.G. Effect of early-strength polycarboxylate superplasticizer on early hydration of reference cement. *Bull. Chin. Ceram. Soc.* **2022**, *41*, 1211–1221.
22. Honorio, T.; Benboudjema, F.; Bore, T.; Ferhat, M.; Vourc'h, E. The pore solution of cement-based materials: Structure and dynamics of water and ions from molecular simulations. *Phys. Chem. Chem. Phys.* **2019**, *21*, 11111–11121. [[CrossRef](#)] [[PubMed](#)]
23. Honorio, T.; Carasek, H.; Cascudo, O. May self-diffusion of ions computed from molecular dynamics explain the electrical conductivity of pore solutions in cement-based materials? *Mater. Struct.* **2020**, *53*, 1–13. [[CrossRef](#)]
24. Honorio, T.; Thierry, B.; Benboudjema, F.; Vourc'h, E.; Ferhat, M. Dielectric properties of the pore solution in cement-based materials. *J. Mol. Liq.* **2020**, *302*, 112548. [[CrossRef](#)]
25. Lothenbach, B.; le Saout, G.; Gallucci, E.; Scrivener, K.L. Influence of limestone on the hydration of Portland cements. *Cem. Concr. Res.* **2008**, *38*, 848–860. [[CrossRef](#)]
26. Heikal, M.; Morsy, M.S.; Aiad, I. Effect of treatment temperature on the early hydration characteristics of superplasticized silica fume blended cement pastes. *Cem. Concr. Res.* **2005**, *35*, 680–687. [[CrossRef](#)]
27. Gao, J.M.; Qian, C.X.; Wang, B.; Morino, K. Experimental study on properties of polymer-modified cement mortars with silica fume. *Cem. Concr. Res.* **2002**, *32*, 41–45. [[CrossRef](#)]
28. Li, H.; Farzadnia, N.; Shi, C. The role of seawater in interaction of slag and silica fume with cement in low water-to-binder ratio pastes at the early age of hydration. *Constr. Build. Mater.* **2018**, *185*, 508–518. [[CrossRef](#)]
29. Wang, C.L.; Liu, Z.P.; Zhang, T.T.; Zhang, Y.; Liu, Z.; Zhao, X. Influence of the Concentration of Seawater on the Early Hydration Properties of Calcium Sulphoaluminate (CSA) Cement: A Preliminary Study. *Buildings* **2021**, *11*, 243. [[CrossRef](#)]
30. Cao, Y.Z.; Guo, L.P.; Chen, B.; Fei, X. Modeling early age hydration kinetics and the hydrated phase of cement paste blended with chloride and sulfate. *Constr. Build. Mater.* **2020**, *261*, 120537. [[CrossRef](#)]
31. Juenger, M.C.G.; Monteiro, P.J.M.; Gartenr, E.M.; Denbeaux, G.P. A soft X-ray microscope investigation into the effects of calcium chloride on tricalcium silicate hydration. *Cem. Concr. Res.* **2005**, *35*, 19–25. [[CrossRef](#)]
32. Cao, Z.Y.; Guo, L.P.; Xue, X.L. Effect of sodium chloride and sodium sulfate on hydration process. *J. Southeast Univ. Nat. Sci. Ed.* **2019**, *49*, 712–719.
33. Shi, C.J.; Day, R.L. Pozzolanic reaction in the presence of chemical activators: Part I. Reaction kinetics. *Cem. Concr. Res.* **2000**, *30*, 51–58. [[CrossRef](#)]

34. Zhang, Y.; Shi, M.L. Study of the hydration process of cement-based materials by AC impedance technique. *J. Build. Mater.* **2000**, *2*, 109–112.
35. Zhang, G.F.; Wang, P.M. Study of hydration process of cement paste modified with hydroxyethyl methyl cellulose by AC impedance spectroscopy. *J. Build. Mater.* **2014**, *17*, 9–14.
36. Lagier, F.; Kurtis, K.E. Influence of Portland cement composition on early age reactions with metakaolin. *Cem. Concr. Res.* **2007**, *37*, 1411–1417. [[CrossRef](#)]
37. Reches, Y. Nanoparticles as concrete additives: Review and perspectives. *Constr. Build. Mater.* **2018**, *175*, 483–495. [[CrossRef](#)]
38. Hwang, J.H. Impedance Spectroscopy Analysis of Hydration in Ordinary Portland Cements Involving Chemical Mechanical Planarization Slurry. *J. Korean Ceram. Soc.* **2012**, *49*, 260–265. [[CrossRef](#)]
39. Zhan, P.M.; He, Z.H.; Ma, Z.M.; Zhang, X.; Abreham, A.A.; Shie, J. Utilization of nano-metakaolin in concrete: A review. *J. Build. Eng.* **2020**, *30*, 101259. [[CrossRef](#)]
40. Li, Q.C.; Fan, Y.F. Effect of nano-metakaolin on the thixotropy of fresh cement paste. *Constr. Build. Mater.* **2022**, *353*, 129062. [[CrossRef](#)]
41. Roussel, N. A thixotropy model for fresh fluid concretes: Theory, validation and applications. *Cem. Concr. Res.* **2006**, *36*, 1797–1806. [[CrossRef](#)]
42. Li, Q.C.; Fan, Y.F. Rheological evaluation of nano-metakaolin cement pastes based on the water film thickness. *Constr. Build. Mater.* **2022**, *324*, 126517. [[CrossRef](#)]
43. Wang, Q.; Cui, X.Y.; Wang, J.; Lv, C.; Dong, Y. Effect of fly ash on rheological properties of graphene oxide cement paste. *Constr. Build. Mater.* **2017**, *138*, 35–44. [[CrossRef](#)]
44. El-Hadj, K.; Said, K.; Karim, E.; Siddique, R.; De Schuttere, G. Influence of metakaolin and silica fume on the heat of hydration and compressive strength development of mortar. *Appl. Clay. Sci.* **2011**, *53*, 704–708.
45. Kawashima, S.; Wang, K.J.; Ferron, R.D.; Kim, J.H.; Tregger, N.; Shah, S. A review of the effect of nanoclays on the fresh and hardened properties of cement-based materials. *Cem. Concr. Res.* **2021**, *147*, 106502. [[CrossRef](#)]
46. Wang, Y.Y.; Zhao, L.H.; Zhao, J. Effects of submicron metakaolin on hydration and compressive strength of portland cement slurry. *KSCE J. Civ. Eng.* **2021**, *25*, 2631–2639. [[CrossRef](#)]